Electronic Supplementary Material (ESI) for Journal of Materials Chemistry A.

Nanoporous metal phosphide catalyst for bifunctional water splitting

Wence Xu,[1] Shengli Zhu,[,1,2,3] Yanqin Liang,[1,2] Zhenduo Cui,[1] Xianjin Yang,[1,2] Akihisa Inoue[1,4]*

[1] School of Materials Science and Engineering, Tianjin University, Tianjin, 300072, China

[2] Tianjin Key Laboratory of Composite and Functional Materials, Tianjin, 300072, China

[3] Key Laboratory of Advanced Ceramics and Mchining Technology, Ministry of Education, Tianjin, 300072, China

[4] Department of Physics, Kings Abudulaziz University, 22254, Jeddah, Saudi Arabia

1. Material and methods

1.1 Preparation of the np-$(Ni_xFe_{1-x})_4P_5$ materials.

The np-$(Ni_xFe_{1-x})_4P_5$ materials were fabricated by electrochemical dealloying amorphous $Ni_yFe_{80-y}P_{20}$ (y=70, 65, 60) alloys. The amorphous $Ni_yFe_{80-y}P_{20}$ alloys were prepared by melt-spinning method [1]. Briefly, pure Ni, Fe, Fe_3P and Ni_2P with controlled proportion were melted into alloy ingots three times under argon atmosphere in a high frequency melting furnace. Then the alloy ingots were remelted in quartz tubes and ejected onto a Cu wheel rotating for rapid solidification to form the precursor alloys. The dealloying process was proceeded in a standard three electrode system with saturated calomel electrode (SCE) and platinum electrode as reference electrode and counter electrode, respectively. The as-prepared ribbons were cut into 40 mm × 1 mm × 25 μm. Since the widths of all the part in the ribbon are almost the same (1 mm), we measured 0.5 cm as the working part and the part above the working part was wrapped by Teflon tape. The Teflon tape was pressed along the edge to make sure the electrolyte can not infiltrate into the Teflon tape. Hence the working area for the corrosion part of the two-sides ribbon is 0.1 cm^2. The precursor alloys were etched under 0.2 V vs SCE in 1 M HCl for 20000 s. After dealloying, the as-prepared samples were then washed in deionized water and ethyl alcohol in sequence then dried in vacuum oven at 30 °C for 12 h. For np-Ni_4P_5 sample, the fabrication process is similar to the np-$(Ni_xFe_{1-x})_4P_5$, the precursor alloy is $Ni_{70}Mn_{10}P_{20}$ alloy because it is hard to fabricate np-Ni_4P_5 from Ni-P precursor alloy due to the strong corrosion resistance for Ni-P amorphous alloy.

The crystalline np-$(Ni_{0.67}Fe_{0.33})_4P_5$ was prepared by annealing amorphous np-$(Ni_{0.67}Fe_{0.33})_4P_5$ at 450 °C for 5 min under an Ar atmosphere.

1.2 Characterization.

Field emission scanning electron microscopy (FESEM, Hitachi S-4800) and Transmission Electron Microscope (TEM, JEOL) were used to characterize the morphologies of the as-prepared materials. X-ray diffraction (XRD) patterns were recorded by Bruker D8 instrument with a Cu Kα radiation source. X-ray photoelectron spectroscopy was performed on PHL1600ESCA. Crystallization behaviors were studied by differential scanning calorimetry (DSC; Perkin Elmer DSC 7, Norwalk, CT) from 50 degrees to 600 degrees at a heating rate of 40 K min^{-1}.

1.3 Electrochemical measurement.

Electrochemical measurements were performed on an electrochemical workstation (Gamry Interface 1000). A typical three electrode system was used in 1 M KOH aqueous solution. The reference electrode and counter electrode were the SCE and carbon rod, respectively. Commercial Pt/C and Ir/C catalysts powder were used as control group. The ink of these catalysts were typically made by dispersing 4 mg catalyst in 1000 μL water/ethanol mixture with a volume ratio of 4:1. Then 80 μL of 5 wt.% of Nafion solution was added to the ink and mixed under ultrasonication. 50 μL ink was pipetted onto the glassy carbon electrode (GCE, 0.2826 cm^{-2}). Then the as-prepared electrode was dried in vacuum oven at 30 °C for 5 h. Due to the as-prepared samples maintain the shape of the original precursor alloy, they can be used directly as the working electrode. For the np-$(Ni_xFe_{1-x})_4P_5$ materials, the corrosion part

of the ribbons were used as the testing part, the area of the testing parts were 0.1 cm^2. The 10th cycle of the polarization curves were used to compare the electrocatalytic activity for each sample. All the potentials were calculated to the reversible hydrogen electrode (RHE) according to the equation (1):

$$E_{(RHE)} = E_{(SCE)} + 0.2412 + 0.059\,pH \quad (1)$$

Before measurement, the electrolyte was degassed by bubbling nitrogen gas for 30 min. The scan rate of the polarization measurement was 2 mV s^{-1}, and the test temperature was 25 °C. The polarization curve was *iR*-compensated according to the following equation:

$$E_{corr} = E_{mea} - iR_s \quad (2)$$

Where E_{corr} is the *iR*-compensated potential, E_{mea} is the measured potential, i is the current and R_s is the equivalent series resistance measured by electrochemical impedance spectroscopy (EIS).

Electrochemical active surface measurements were performed by measuring double-layer capacitance (C_{dl}) from the CV curves from 0.97 V to 1.07 V vs RHE at different scan rates. By plotting the $\Delta J = (J_f - J_r)$ at 1.02 V vs RHE against the scan rate, the linear slope that is twice the C_{dl} can be obtained, and is normally used to represent the corresponding ECSA, and assuming a specific capacitance of 40 μF cm^{-2} for a flat surface in according to previous literatures [2, 3]. EIS measurements were carried out at an overpotential of 300 mV and 200 mV for OER and HER, respectively, in the frequency range from 100000 Hz to 0.01 Hz at a perturbation AC voltage of 10 mV. For the aging process, CV measurement with a scan rate of 5 mV s^{-}

[1] was proceeded. The stability measurements were carried under static current density of -10 mA cm^{-2} and 10 mA cm^{-2} for HER and OER, respectively. For the overall water splitting measurements, the electrodes were served as both anode and cathode. The scan rate of the polarization curve was 2 mV s^{-1}. The chronoamperometry stability measurement was carried out under 10 mA cm^{-2} for 20 h.

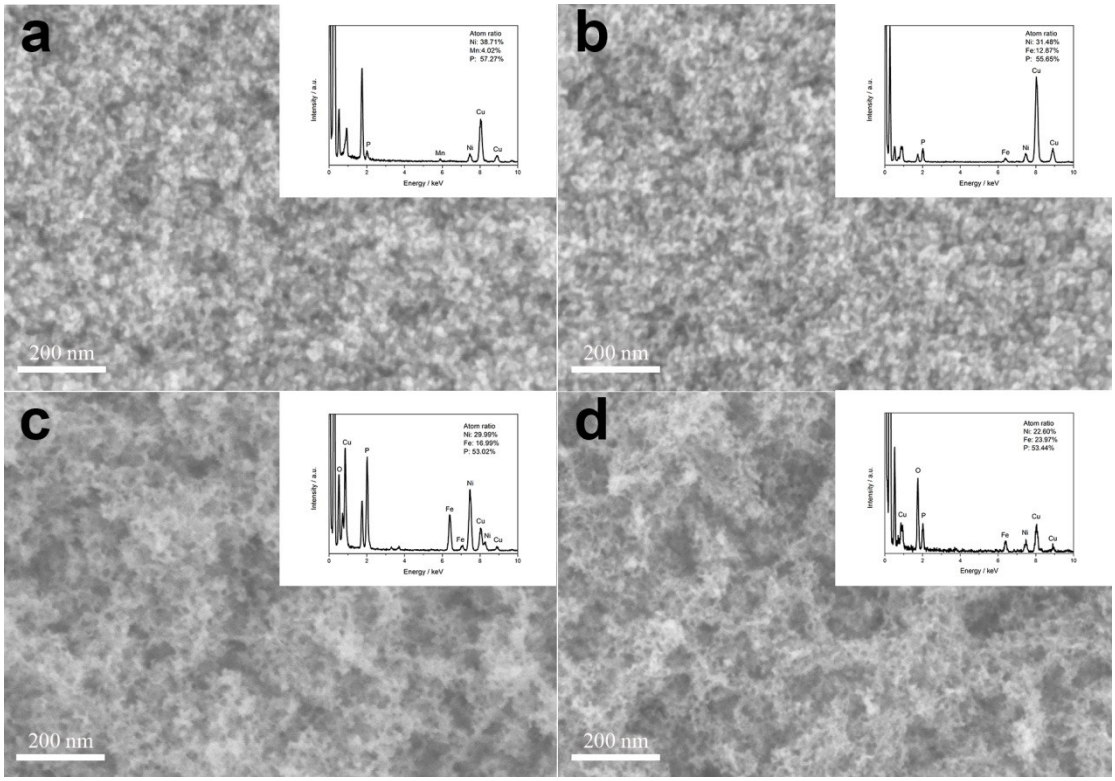

Figure S1. SEM images and EDX spectra (inset) of the np-Ni_4P_5 (a), np-$(Ni_{0.75}Fe_{0.25})_4P_5$ (b), np-$(Ni_{0.67}Fe_{0.33})_4P_5$ (c) and np-$(Ni_{0.5}Fe_{0.5})_4P_5$ (d).

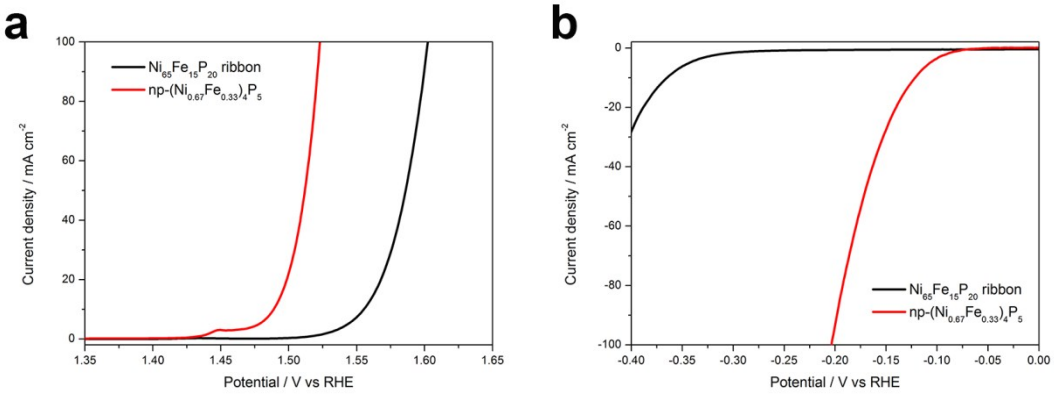

Figure S2 . Polarization curves of the np-$(Ni_{0.67}Fe_{0.33})_4P_5$ and corresponding precursor alloy.

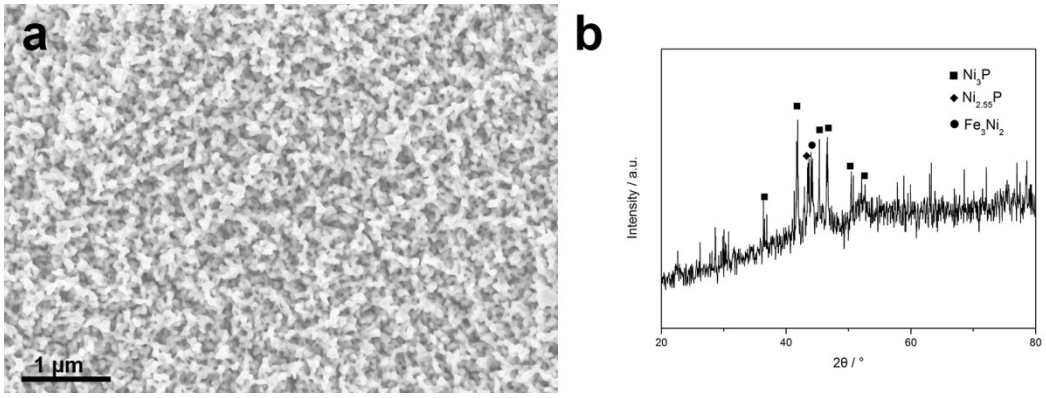

Figure S3. SEM image (a) and XRD pattern (b) of the np-$(Ni_{0.67}Fe_{0.33})_4P_5$ after annealing.

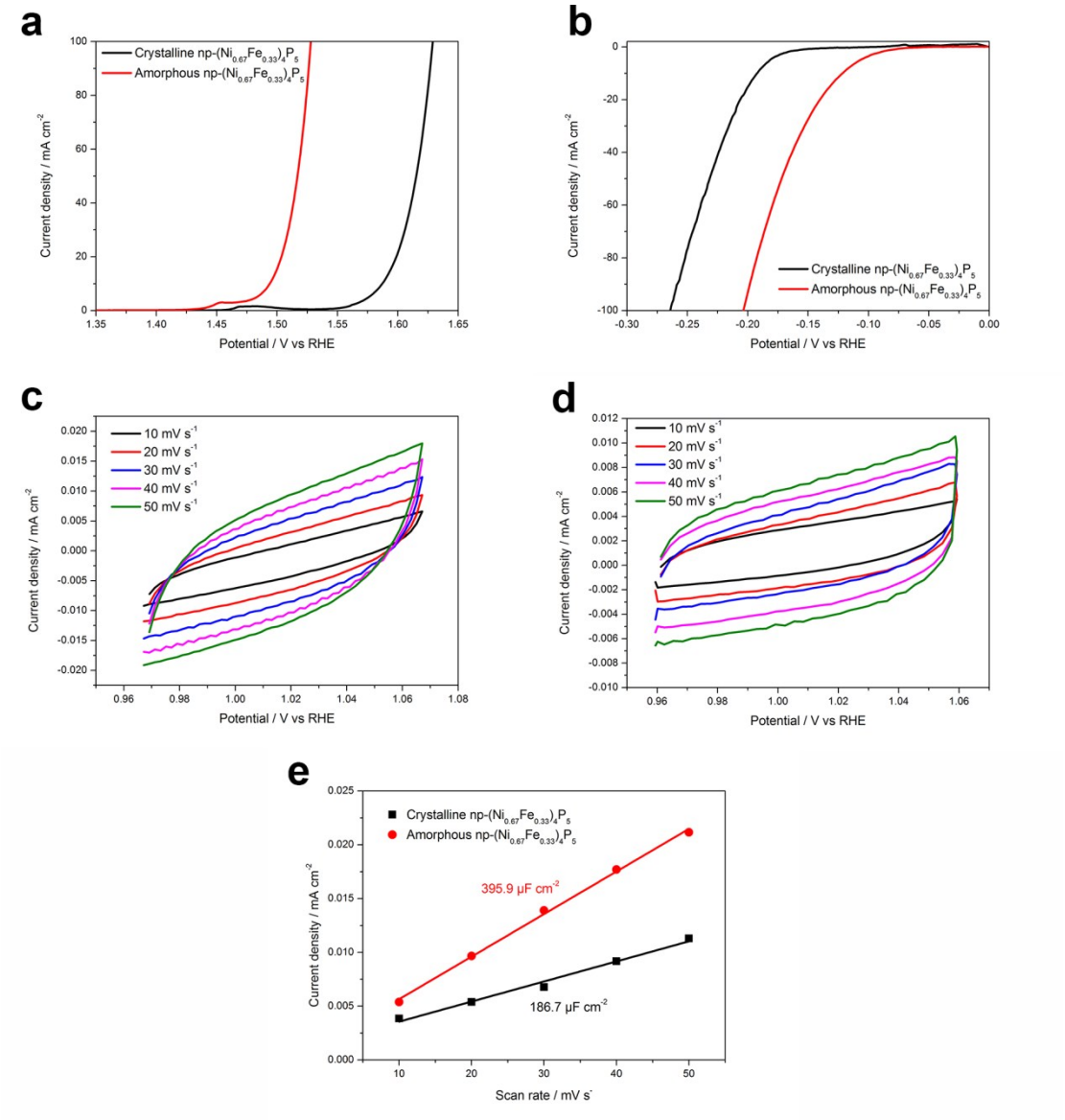

Figure S4. Polarization curves of the amorphous and crystalline np-$(Ni_{0.67}Fe_{0.33})_4P_5$ for OER (a) and HER (b). CV curves of the amorphous (c) and crystalline (d) np-$(Ni_{0.67}Fe_{0.33})_4P_5$ at different scan rate. (e) Corresponding plots showing the extraction of the double layer capacitance for amorphous and crystalline np-$(Ni_{0.67}Fe_{0.33})_4P_5$.

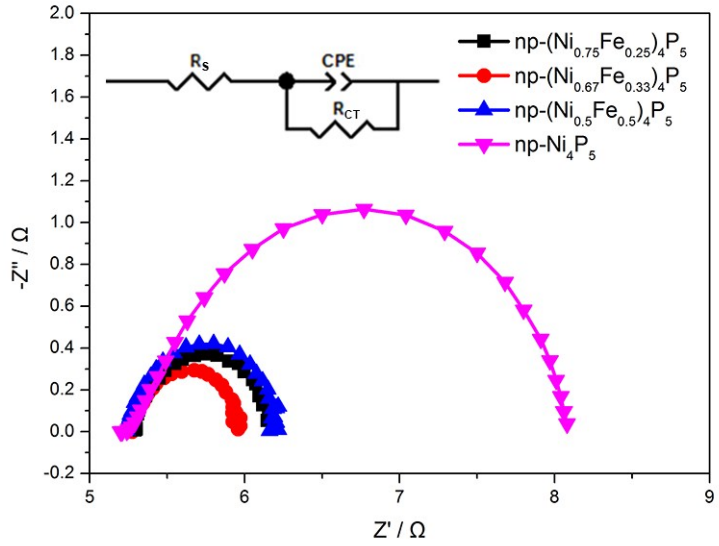

Figure S5. EIS curves of the np-$(Ni_yFe_{1-y})_4P_5$ for OER.

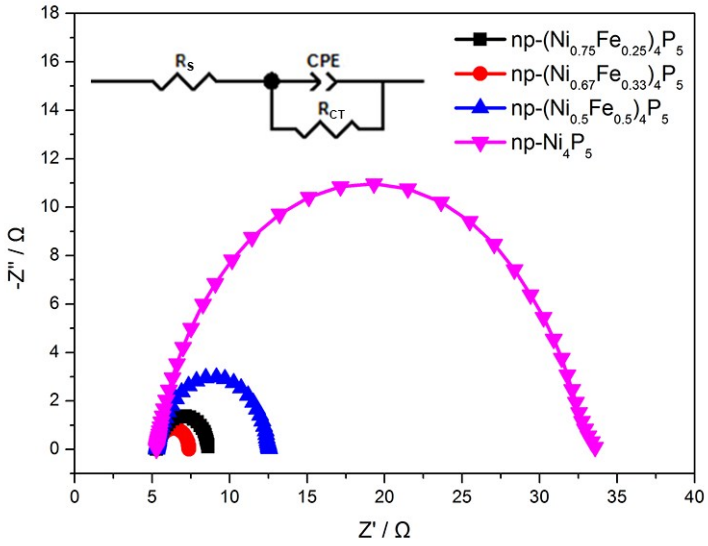

Figure S6. EIS curves of the np-$(Ni_yFe_{1-y})_4P_5$ for HER.

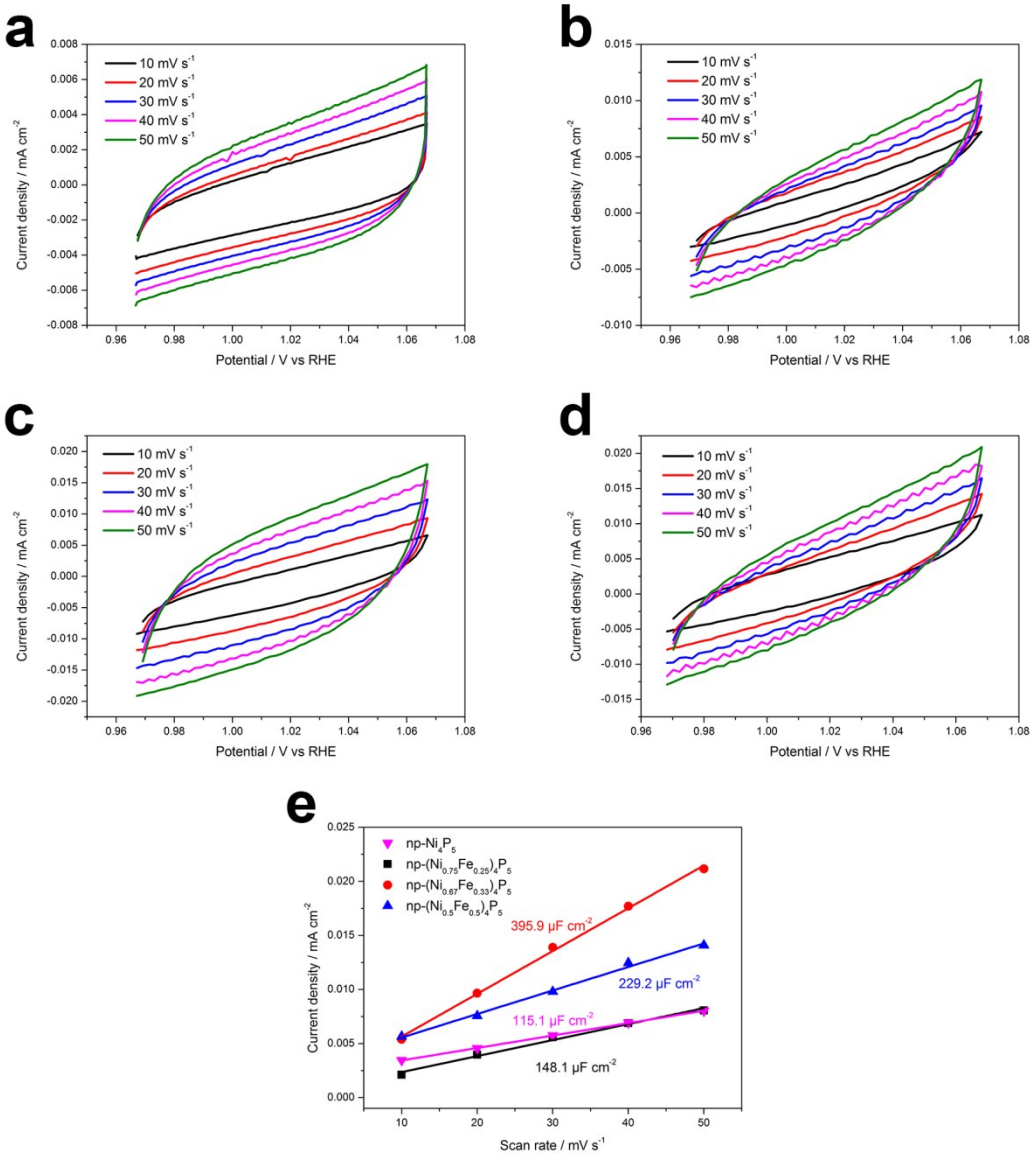

Figure S7. CV curves and corresponding plots showing the extraction of the double layer capacitance for np-$(Ni_yFe_{1-y})_4P_5$.

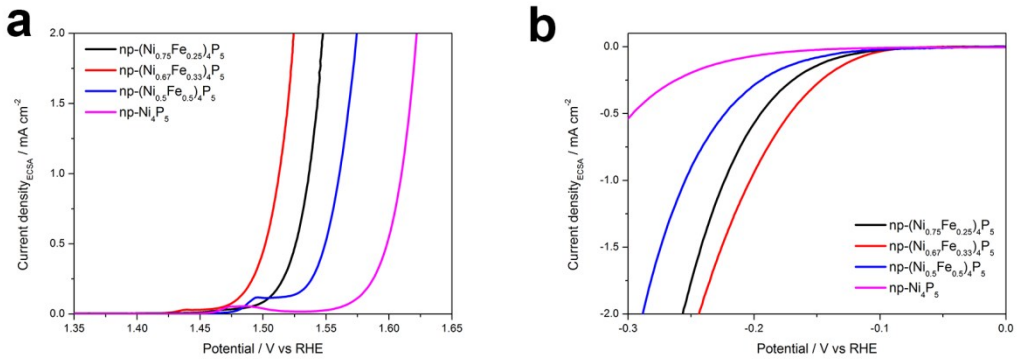

Figure S8. Polarization curves normalized by ECSA of the np-$(Ni_yFe_{1-y})_4P_5$ for OER (a) and HER (b).

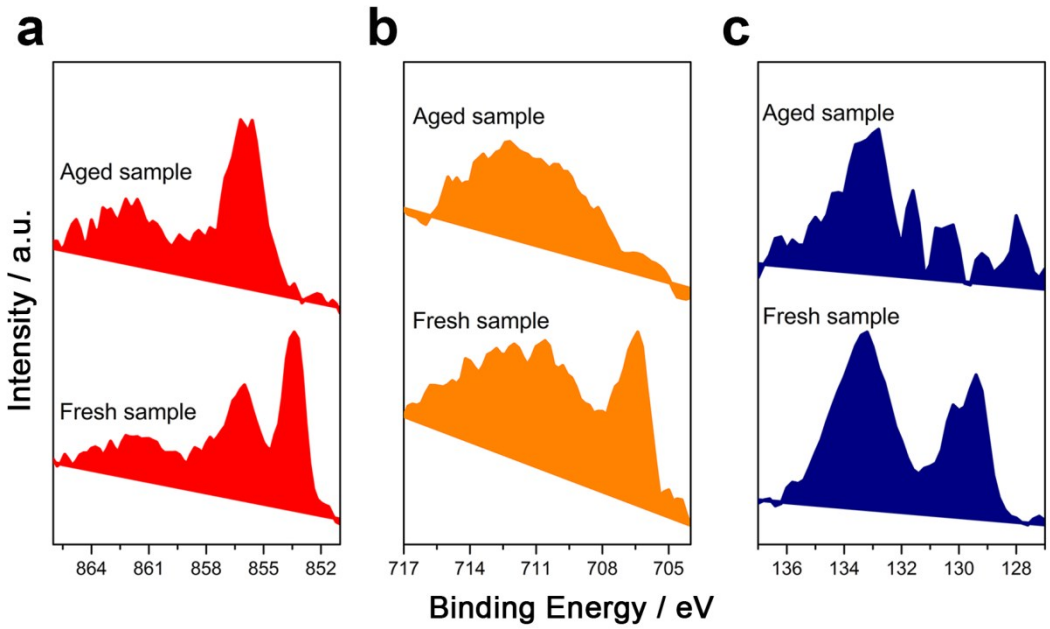

Figure S9. Ni 2p (a), Fe 2p (b) and P 2p (c) spectra of the fresh and aged np-$(Ni_{0.67}Fe_{0.33})_4P_5$.

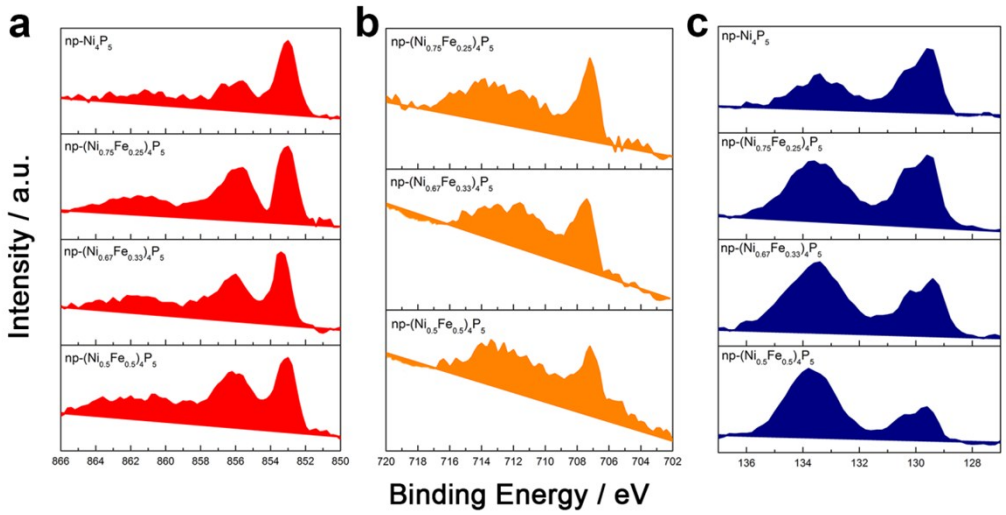

Figure S10. Ni 2p (a), Fe 2p (b) and P 2p (c) spectra of the np-$(Ni_yFe_{1-y})_4P_5$.

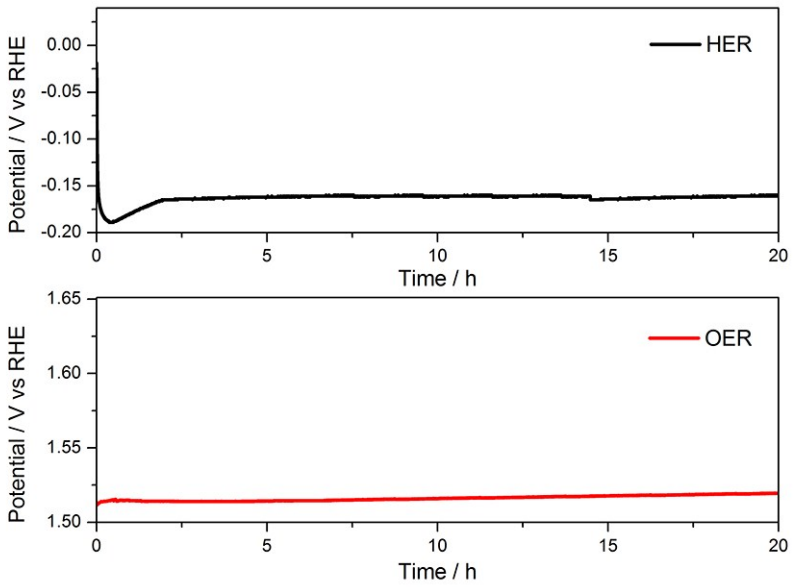

Figure S11. Chronoamperometry curves of the np-$(Ni_{0.67}Fe_{0.33})_4P_5$ for HER and OER.

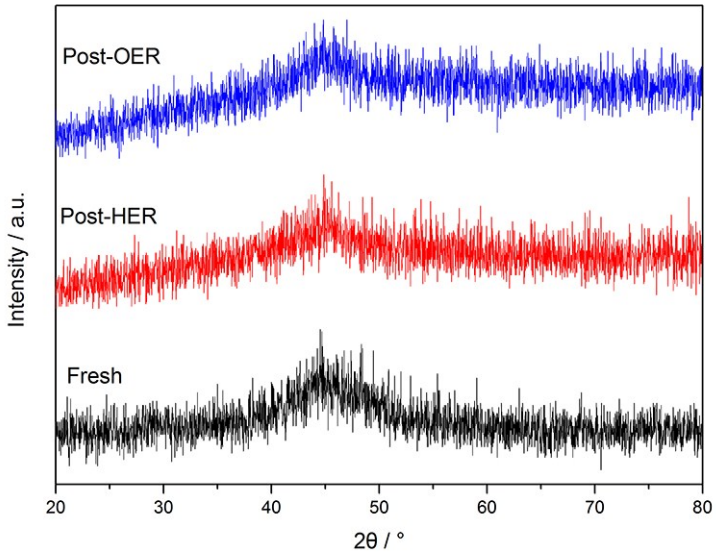

Figure S12. XRD pattern of the fresh, post-HER and post-HER np-$(Ni_{0.67}Fe_{0.33})_4P_5$.

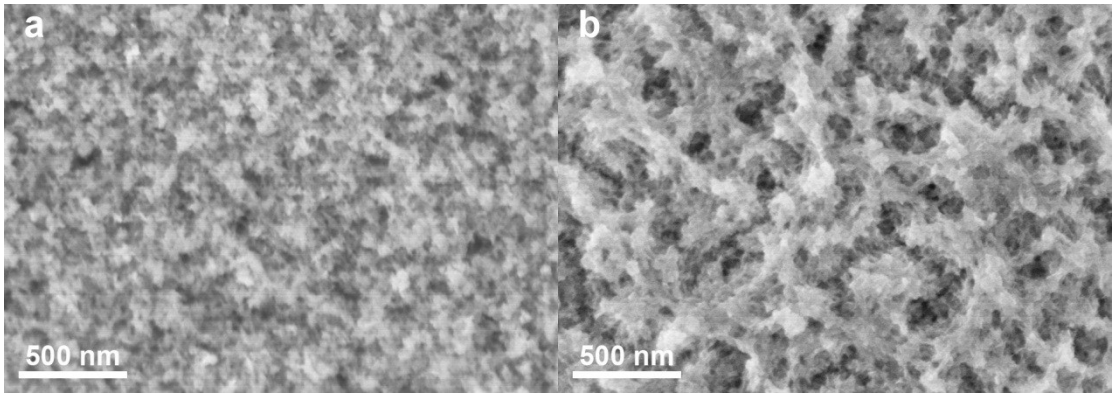

Figure S13. SEM images of the post-HER (a) and post-OER (b) np-$(Ni_{0.67}Fe_{0.33})_4P_5$.

Table S1. Detailed composition of the as-prepared samples

Sample	Ni (%)	Fe (%)	P (%)	Precursor alloy
np-Ni_4P_5	40.33	-	59.67	$Ni_{70}Mn_{10}P_{20}$
np-$(Ni_{0.75}Fe_{0.25})_4P_5$	31.48	12.87	55.65	$Ni_{70}Fe_{10}P_{20}$
np-$(Ni_{0.67}Fe_{0.33})_4P_5$	29.99	16.99	53.02	$Ni_{65}Fe_{15}P_{20}$
np-$(Ni_{0.5}Fe_{0.5})_4P_5$	22.60	23.97	53.44	$Ni_{60}Fe_{20}P_{20}$

Table S2. Summary of the electrocatalytic properties of as-prepared catalysts and other recently reported Ni, Fe based high performance OER catalysts in KOH.

Catalyst	Electrolyte	η_{10} (mV)	Tafel slope (mV dec^{-1})	Substrate	Reference
NiFeP	1 M KOH	277	83	NiFe	4
NiFe-LDH	1 M KOH	230	42	glassy carbon	5
NiFe-LDH	1 M KOH		86	exfoliated graphene	6
NiFeOx	1 M KOH	260	40	Nickel foam	7
NiFeOOH	1 M KOH	280	40	gold	8
NiFe LDH	1 M KOH		40	glassy carbon	9
NiFeOx	1 M KOH			glassy carbon	10
Fe-Ni_3S_2/FeNi	1 M KOH	282	54	NiFe	11
Ni_3FeN/NRGO	0.1 M KOH	400	-	glassy carbon	12
NiFe@NC	1 M KOH	350	56	glassy carbon	13
Ni_3FeN-NPs	1 M KOH	280	46	glassy carbon	14
$Ni_{1-x}Fe_x$/NC	1 M KOH	330	45	glassy carbon	15
Ni−Fe−P	1 M KOH	271	53	glassy carbon	16
$Ni_{1.85}Fe_{0.15}P$ NSAs/NF	1 M KOH	270	96	Nickel foam	17
NiFe-NC	1 M KOH	271	48	Carbon fiber paper	18
Ni-Fe LDHs	1 M KOH	239	-	glassy carbon	19
np-Ni_4P_5	1 M KOH	362	40.9	-	This work
np-$(Ni_{0.75}Fe_{0.25})_4P_5$	1 M KOH	280	33.7	-	This work
np-$(Ni_{0.67}Fe_{0.33})_4P_5$	1 M KOH	245	32.9	-	This work
np-$(Ni_{0.5}Fe_{0.5})_4P_5$	1 M KOH	310	37.5	-	This work

Table S3. Summary of the electrocatalytic properties of as-prepared catalysts and other recently reported Ni, Fe based high performance HER catalysts in KOH.

Catalyst	Electrolyte	η_{10} (mV)	Tafel slope (mV dec^{-1})	Substrate	Reference
Fe–NiS_2	0.5 M H_2SO_4	121	37	glassy carbon	20
FeCo@NCNTs	0.1 M H_2SO_4	~300	72	glassy carbon	21
$Ni_{1.5}Fe_{0.5}P$	1 M KOH	282	125	Carbon fiber paper	22
$Ni_{1.5}Fe_{0.5}P$/CF	1 M KOH	158	-	Carbon fiber paper	22
NiFe@NC	1 M KOH	~240	-	glassy carbon	13
Ni_3FeN-NPs	1 M KOH	158	42	glassy carbon	14
$Ni_{1-x}Fe_x$/NC	1 M KOH	219	101	glassy carbon	15
NiFeS/NF	1 M KOH	180	53	Nickel foam	23
Ni−Fe−P	1 M KOH	182	85	glassy carbon	16
$Ni_{1.85}Fe_{0.15}P$ NSAs/NF	1 M KOH	106	89.7	Nickel foam	17
NiFe-NC	1 M KOH	197	130	Carbon fiber paper	18
np-Ni_4P_5	1 M KOH	278	109.4	-	This work
np-$(Ni_{0.75}Fe_{0.25})_4P_5$	1 M KOH	157	66.5	-	This work
np-$(Ni_{0.67}Fe_{0.33})_4P_5$	1 M KOH	120	41.8	-	This work
np-$(Ni_{0.5}Fe_{0.5})_4P_5$	1 M KOH	198	86.2	-	This work

Table S4. Fitting parameters of the np-$(Ni_yFe_{1-y})_4P_5$ for OER.

Sample	R_S (Ω)	CPE	n	R_{CT} (Ω)
np-$(Ni_{0.75}Fe_{0.25})_4P_5$	5.289	0.01536	0.8786	0.88764
	(0.09939%) [a]	(3.9332%)	(0.73131%)	(0.47657%)
np-$(Ni_{0.67}Fe_{0.33})_4P_5$	5.312	0.00988	0.84052	0.7493
	(0.08577%)	(3.5312%)	(0.75438%)	(0.49258%)
np-$(Ni_{0.5}Fe_{0.5})_4P_5$	5.291	0.00349	0.88799	0.99197
	(0.07755%)	(3.1985%)	(0.67652%)	(0.43651%)
np-Ni_4P_5	5.277	6.36E-04	0.90125	2.879
	(0.09082%)	(3.3731%)	(0.78181%)	(0.51572%)

[a] The values in the round brackets are the fitting errors.

Table S5. Fitting parameters of the np-$(Ni_yFe_{1-y})_4P_5$ for HER.

Sample	R_S (Ω)	CPE	n	R_{CT} (Ω)
np-$(Ni_{0.75}Fe_{0.25})_4P_5$	5.298	9.11E-04	0.87793	3.356
	(0.08923%) [a]	(2.9792%)	(0.63132%)	(0.49659%)
np-$(Ni_{0.67}Fe_{0.33})_4P_5$	5.304	7.28E-04	0.89012	2.078
	(0.09636%)	(3.3732%)	(0.77431%)	(0.43527%)
np-$(Ni_{0.5}Fe_{0.5})_4P_5$	5.287	0.00116	0.86032	7.481
	(0.08163%)	(3.1398%)	(0.72231%)	(0.42658%)
np-Ni_4P_5	5.281	0.00127	0.85469	28.89
	(0.09379%)	(3.6338%)	(0.73831%)	(0.47935%)

[a] The values in the round brackets are the fitting errors.

Table S6. Summary of the electrocatalytic properties of as-prepared catalysts and other recently reported Ni, Fe based high performance bifunctional catalysts in KOH.

Catalyst	Electrolyte	η_{10} (mV)	Substrate	Reference
NiFe@NC	1 M KOH	580	glassy carbon	[13]
NiFe HNSs	1 M KOH	440	glassy carbon	[24]
$Ni_{1.5}Fe_{0.5}P$/CF	1 M KOH	359	Carbon fiber paper	[22]
NiFe/$NiCo_2O_4$/Ni	1 M KOH	440	Nickel foam	[25]
$FeNi_3N$/NF	1 M KOH	390	Nickel foam	[26]
$Ni_{1-x}Fe_x$/NC	1 M KOH	410	glassy carbon	[15]
Ni−Fe−P	1 M KOH	440	glassy carbon	[16]
$Ni_{1.85}Fe_{0.15}P$ NSAs/NF	1 M KOH	380	Nickel foam	[17]
NiFe-NC	1 M KOH	440	Carbon fiber paper	[18]
np-$(Ni_{0.67}Fe_{0.33})_4P_5$	1 M KOH	390	-	This work

Reference

1. S. L. Zhu, J. L. He, X. J. Yang, Z. D. Cui and L. L. Pi, *Electrochem. Commun.*, 2011, **13**, 250.
2. X. Zhang, X. Zhang, H. Xu, Z. Wu, H. Wang and Y. Liang, *Adv. Funct. Mater.* 2017, **27**, 1606635.
3. C. C. L. McCrory, S. Jung, I. M. Ferrer, S. M. Chatman, J. C. Peters and T. F. Jaramillo, *J. Am. Chem. Soc.*, 2015, **137**, 4347.
4. C. G. Read, J. F. Callejas, C. F. Holder and R. E. Schaak, *ACS Appl. Mat. Interfaces*, 2016, **8**, 12798.
5. W. Ma, R. Ma, C. Wang, J. Liang, X. Liu, K. Zhou and T. Sasaki, *ACS Nano*, 2015, **9**, 1977.
6. Y. Hou, M. R. Lohe, J. Zhang, S. Liu, X. Zhuang and X. Feng, *Energy Environ. Sci.*, 2016, **9**, 478.
7. E. Nurlaela, T. Shinagawa, M. Qureshi, D. S. Dhawale and K. Takanabe, *ACS Catal.*, 2016, **6**, 1713.
8. M. W. Louie and A. T. Bell, *J. Am. Chem. Soc.*, 2013, **135**, 12329.
9. F. Song and X. Hu, *Nat. Commun.*, 2014, **5**, 4477.
10. C. C. L. McCrory, S. Jung, J. C. Peters and T. F. Jaramillo, *J. Am. Chem. Soc.*, 2013, **135**, 16977.
11. C.-Z. Yuan, Z.-T. Sun, Y.-F. Jiang, Z.-K. Yang, N. Jiang, Z.-W. Zhao, U. Y. Qazi, W.-H. Zhang and A.-W. Xu, *Small*, 2017, **13**, 1604161.
12. Y. Fan, S. Ida, A. Staykov, T. Akbay, H. Hagiwara, J. Matsuda, K. Kaneko and T. Ishihara, *Small*, 2017, **13**, 1700099.
13. Z. Zhang, Y. Qin, M. Dou, J. Ji and F. Wang, *Nano Energy*, 2016, **30**, 426.
14. X. Jia, Y. Zhao, G. Chen, L. Shang, R. Shi, X. Kang, G. I. N. Waterhouse, L.-Z. Wu, C.-H. Tung and T. Zhang, *Adv. Energy. Mater.*, 2016, **6**, 1502585.

15. X. Zhang, H. Xu, X. Li, Y. Li, T. Yang and Y. Liang, *ACS Catal.*, 2016, **6**, 580.
16. C. Xuan, J. Wang, W. Xia, Z. Peng, Z. Wu, W. Lei, K. Xia, H. L. Xin and D. Wang, *ACS Appl. Mat. Interfaces,* 2017, **9**, 26134-26142.
17. P. Wang, Z. Pu, Y. Li, L. Wu, Z. Tu, M. Jiang, Z. Kou, I. S. Arniinu and S. Mu, *ACS Appl. Mat. Interfaces*, 2017, **9**, 26001-26007.
18. A. Kumar and S. Bhattacharyya, *ACS Appl. Mat. Interfaces*, 2017, **9**, 41906-41915.
19. K. Zhang, W. Wang, L. Kuai and B. Geng, *Electrochim. Acta*, 2017, **225**, 303-309.
20. J. Yan, H. Wu, P. Li, H. Chen, R. Jiang and S. Liu, *J. Mater. Chem. A*, 2017, **5**, 10173.
21. J. Deng, P. Ren, D. Deng, L. Yu, F. Yang and X. Bao, *Energy Environ. Sci.*, 2014, **7**, 1919.
22. H. Huang, C. Yu, C. Zhao, X. Han, J. Yang, Z. Liu, S. Li, M. Zhang and J. Qiu, *Nano Energy*, 2017, **34**, 472.
23. P. Ganesan, A. Sivanantham and S. Shanmugam, *J. Mater. Chem. A*, 2016, **4**, 16394.
24. X. Sun, Q. Shao, Y. Pi, J. Guo and X. Huang, *J. Mater. Chem. A*, 2017, **5**, 7769.
25. C. Xiao, Y. Li, X. Lu and C. Zhao, *Adv. Funct. Mater.* 2016, **26**, 3515.
26. B. Zhang, C. Xiao, S. Xie, J. Liang, X. Chen and Y. Tang, *Chem. Mater.*, 2016, **28**, 6934.